Effects of gas pressure on plasma characteristics in dual frequency argon capacitive glow discharges at low pressure by a self-consistent fluid model*

Lu-Lu Zhao(赵璐璐)[1,2], Yue Liu(刘悦)[1,†], and Tagra Samir[1]

[1] *Key Laboratory of Materials Modification by Laser, Ion and Electron Beams (Ministry of Education), School of Physics, Dalian University of Technology, Dalian* 116024, *China*

[2] *School of Information Science and Engineering, Dalian Polytechnic University, Dalian* 116034, *China*

(Received 29 June 2017; revised manuscript received 30 August 2017; published online 20 October 2017)

A self-consistent fluid model for dual radio frequency argon capacitive glow discharges at low pressure is established. Numerical results are obtained by using a finite difference method to solve the model numerically, and the results are analyzed to study the effect of gas pressure on the plasma characteristics. It shows that when the gas pressure increases from 0.3 Torr (1 Torr = 1.33322×10^2 Pa) to 1.5 Torr, the cycle-averaged plasma density and the ionization rate increase; the cycle-averaged ion current densities and ion energy densities on the electrodes electrode increase; the cycle-averaged electron temperature decreases. Also, the instantaneous electron density in the powered sheath region is presented and discussed. The cycle-averaged electric field has a complex behavior with the increasing of gas pressure, and its changes take place mainly in the two sheath regions. The cycle-averaged electron pressure heating, electron ohmic heating, electron heating, and electron energy loss are all influenced by the gas pressure. Two peaks of the electron heating appear in the sheath regions and the two peaks become larger and move to electrodes as the gas pressure increases.

Keywords: dual frequency, gas pressure, glow discharge

PACS: 52.25.Jm, 52.30.Ex, 52.50.Qt, 52.65.–y **DOI:** 10.1088/1674-1056/26/12/125201

1. Introduction

In traditional single frequency capacitively coupled plasma (CCP), it is difficult to control plasma density and ion energy separately. The independent controlling of the ion flux and bombarding energy can be easily achieved in a dual frequency CCPs system. They have been widely used in many applications, such as plasma etching, deposition and surface modification.[1–5] In the dual frequency discharges, the high frequency controls the ion flux, while the low frequency mainly determines the ion energy. The ion flux and the ion energy play important roles in plasma processing applications.

A significant number of research studies have been done experimentally, theoretically and also by modeling to study dual frequency CCP in order to improve its application efficiency.[6–24] For the dual frequency of (2 + 27) MHz and the gas pressure of 6.7 Pa with silicon electrodes, Kim *et al.* measured the electron density and ion flux. [9] Li *et al.* used a dual frequency CCP device to study the ion energy distributions in Ar/CF_4 plasma.[10] Jiang *et al.* measured the ion density and electron temperature in a dual frequency CCP by using a complete floating double probe technique. Their results indicated an obvious dual frequency modulating effect on the plasma parameters and the spatial distributions of the plasma parameters.[11] Yu *et al.* investigated an argon CCP driven separately by dual frequencies of 13.56/2, 27/2, 41/2, and 60 MHz/2 MHz, by using a floating double electrical probe and optical emission spectroscopy.[12] In the dual frequency CCP driven by 60 MHz/13.56 MHz at low pressure, the effects of low frequency power on the plasma characteristics measured by using a compensated Langmuir electrostatic probe was presented by Yuan *et al.* Their results indicated that the independent controlling of the plasma density and the ion bombardment energy can be achieved at low pressures only.[21] They used the same experimental method to measure the electron energy probability functions in a 60-MHz/13.56-MHz dual frequency CCP. The effects of the gas pressure on the electron density, the effective electron temperature, the floating potential, and the plasma potential in 60-MHz/13.56-MHz dual frequency CCP were measured and compared with those of a 60-MHz single frequency CCP: the results were found to be similar.[22]

Electron heating is the sum of the electron ohmic heating (collisional) and the electron pressure heating (collisionless). The collisionless electron heating is based on a strongly simplified version of the electron momentum balance equation, where inertia terms are ignored. It can contribute to the collisionless electron heating as demonstrated by Laeur *et al.*[25] The phenomenon of collisionless electron heating was described by a mechanism known as the Fermi acceleration and can also be described as an electron pressure heating effect

*Project supported by the National Natural Science Foundation of China (Grant No. 51172101).

†Corresponding author. E-mail: liuyue@dlut.edu.cn

© 2017 Chinese Physical Society and IOP Publishing Ltd

caused by the constant compression and rarefaction of population in the sheath vicinity, as the sheath expands and contracts. Gahan and Hopkins showed that the electrons travelling from the bulk plasma collide with the moving sheath edge and gain or lose energy depending on whether the sheath motion is towards or backward the electrons.[26] For these reasons, studying the effects of gas pressure is important for understanding the basic discharge dynamics and process. In the bulk plasma region, the ohmic heating of electrons due to collisions is no longer sufficient to sustain the plasma effectively. In the sheath region, the collisionless electron heating exists and therefore the electron gains energy through stochastic interaction with the electric field. Turner and Chabert investigated the collisionless electron heating mechanisms with dual frequency. For typical parameters, they found an interesting result that the heating generated from two currents with dual frequency can be much larger than the effect of single frequency.[27] Schulze *et al*. had two separate points for electron heating modes in CCPs.[28] These modes described by Belenguer *et al*. are α-mode and γ-mode. (i) In the α- mode, the ionization is formed by electrons which are accelerated by the oscillating sheath edges. (ii) In the γ-mode, the ionization is formed by secondary electron avalanches.[29]

In our work, the effect of gas pressure on the plasma characteristics in dual frequency argon capacitive glow discharge at low pressure is investigated by a self-consistent fluid model. Since the gap between the electrodes is much smaller than the electrode diameter, a one-dimensional fluid model can describe the plasma successfully.

The rest of this paper is organized as follows. The model is presented in Section 2. In Section 3 , the numerical results are given and discussed for some parameters influenced by gas pressure. Finally, a brief summary and some conclusions are presented in Section 4.

2. Simulation model

As is well known, the main reactions in argon discharge include the grounded state excitation, the grounded state ionization, the step-wise ionization, the superelastic collisions, the quenching to resonance, the metastable pooling, the two-body quenching, and the three-body quenching.[23,30] These reactions are listed in Table 1.

Table 1. Main reactions in argon discharge.[23,30]

	Reaction	Process	H_j/eV	Rate coefficient
1	$e + Ar \rightarrow Ar^* + e$	(ground state excitation)	11.56	$k_{ex} = 3.712 \times 10^{-8} \exp(-15.06/T_e)$
2	$e + Ar \rightarrow Ar^+ + 2e$	(ground state ionization)	15.7	$k_i = 1.235 \times 10^{-7} \exp(-18.687/T_e)$
3	$e + Ar^* \rightarrow Ar^+ + 2e$	(step-wise ionization)	4.14	$k_{sc} = 2.05 \times 10^{-9} \exp(-4.59/T_e)$
4	$e + Ar^* \rightarrow Ar + e$	(superelastic collisions)	–11.56	$k_{sc} = 1.818 \times 10^{-9} \exp(-2.14/T_e)$
5	$e + Ar^* \rightarrow Ar^r + e$	(quenching to resonance)		$k_r = 2 \times 10^{-7}$
6	$Ar^* + Ar^* \rightarrow Ar^+ + Ar + e$	(metastable pooling)		$k_{mp} = 6.2 \times 10^{-10}$
7	$Ar^* + Ar \rightarrow 2Ar$	(two-body quenching)		$k_{2q} = 3.0 \times 10^{-15}$
8	$Ar^* + 2Ar \rightarrow Ar + Ar_2$	(three-body quenching)		$k_{3q} = 1.1 \times 10^{-31}$

A fluid model is employed to describe the plasma in a low pressure dual frequency capacitively coupled discharge. In this model, the densities of ions and electrons between the electrodes satisfy the following continuity equations.[23,24,30]

$$\frac{\partial n_i}{\partial t} + \nabla \cdot \boldsymbol{J}_i = S, \tag{1}$$

$$\frac{\partial n_e}{\partial t} + \nabla \cdot \boldsymbol{J}_e = S, \tag{2}$$

where n_i and n_e represent the number densities of ions and electrons, $\boldsymbol{J}_i$, and $\boldsymbol{J}_e$ denote the fluxes of ions and electrons, respectively. When the effect of the metastable atoms is ignored, only the grounded state ionization needs to be considered so that the source term S can be written as

$$S = k_i n_n n_e, \tag{3}$$

where n_n is the number density of neutral atoms, which can be written as

$$n_n = 3.22 \times 10^{16} p \ (\mathrm{cm}^{-3}), \tag{4}$$

where p is the pressure of the neutral gas in units of Torr. The ionization coefficient k_i can be written as a function of electron temperature[23,24]

$$k_i = k_{i0} \exp(-E_i/T_e), \tag{5}$$

where T_e is the electron temperature in units of eV.

Based on the drift-diffusion approximation, the fluxes of the ions and the electrons are written as

$$\boldsymbol{J}_i = -D_i \nabla n_i + \mu_i n_i \boldsymbol{E}, \tag{6}$$

$$\boldsymbol{J}_e = -D_e \nabla n_e - \mu_e n_e \boldsymbol{E}, \tag{7}$$

where μ_i and μ_e are the mobilities of ions and electrons; D_i and D_e represent the diffusion coefficients of ions and electrons, respectively.

In our model, the energy balance equation for the ions is ignored due to the ion temperature being assumed to be constant. The energy balance for the electrons can be expressed

as

$$\frac{\partial}{\partial t}\left(\frac{3}{2}n_{\mathrm{e}}kT_{\mathrm{e}}\right) = -\nabla\cdot\boldsymbol{q}_{\mathrm{e}} - e\boldsymbol{J}_{\mathrm{e}}\cdot\boldsymbol{E} - H_{\mathrm{i}}S, \tag{8}$$

where k and H_{I} are the Boltzmann constant and the electron energy loss coefficient for ionization, respectively; $\boldsymbol{q}_{\mathrm{e}}$ is the conductive heat flux of electron energy, which can be written as

$$\boldsymbol{q}_{\mathrm{e}} = \frac{5}{2}kT_{\mathrm{e}}\boldsymbol{J}_{\mathrm{e}} - K_{\mathrm{e}}\nabla T_{\mathrm{e}}, \tag{9}$$

where K_{e} is the thermal conductivity which can be expressed as

$$K_{\mathrm{e}} = \frac{3}{2}kD_{\mathrm{e}}n_{\mathrm{e}}. \tag{10}$$

The electric field must satisfy the following equation:

$$\nabla\cdot\boldsymbol{E} = \frac{e}{\varepsilon_0}\left(n_{\mathrm{i}} - n_{\mathrm{e}}\right), \tag{11}$$

where $\boldsymbol{E}$, e and ε_0 are the electric field, the elementary charge, and the permittivity of free space, respectively. The electric field $\boldsymbol{E}$ can be expressed as the negative gradient of the electric potential, i.e.,

$$\boldsymbol{E} = -\nabla V, \tag{12}$$

where V is the electric potential.

In Eq. (8), the term $-e\boldsymbol{J}_{\mathrm{e}}\cdot\boldsymbol{E}$ is called the electron heating, which includes two parts and expressed as

$$p_{\mathrm{c}} = -e\boldsymbol{J}_{\mathrm{e}}\cdot\boldsymbol{E} = p_{\mathrm{p}} + p_{\mathrm{h}}. \tag{13}$$

In which one is the electron pressure heating:

$$p_{\mathrm{p}} = eD_{\mathrm{e}}\boldsymbol{E}\cdot\nabla n_{\mathrm{e}} \tag{14}$$

and the other is the electron ohmic heating:

$$p_{\mathrm{h}} = e\mu_{\mathrm{e}}n_{\mathrm{e}}E^2. \tag{15}$$

In Eq. (8), the term $H_{\mathrm{i}}S$ indicates the electron energy loss:

$$p_{\mathrm{l}} = H_{\mathrm{i}}S. \tag{16}$$

When the sizes of the electrodes are much larger than the gap between them, a one-dimensional model can be used. For the one-dimensional case, the boundary conditions can be expressed below.

At the powered electrode (the left electrode)

$$x = 0: \quad V = V_1\sin\left(2\pi f_1 t\right) + V_2\sin\left(2\pi f_2 t\right), \quad J_{\mathrm{i}} = \mu_{\mathrm{i}}n_{\mathrm{i}}E,$$
$$J_{\mathrm{e}} = -k_{\mathrm{s}}n_{\mathrm{e}} - \gamma J_{\mathrm{i}}, \quad T_{\mathrm{e}} = T_{\mathrm{eb}};$$

at the grounded electrode (the right electrode)

$$x = d: \quad V = 0, \quad J_{\mathrm{i}} = \mu_{\mathrm{i}}n_{\mathrm{i}}E, \quad J_{\mathrm{e}} = k_{\mathrm{s}}n_{\mathrm{e}} - \gamma J_{\mathrm{i}}, \quad T_{\mathrm{e}} = T_{\mathrm{eb}}.$$

The initial condition for the one-dimensional model is as follows:

$$n_{\mathrm{i}} = n_{\mathrm{e}} = n_\varepsilon\left[\varepsilon + 16\left(1-\frac{x}{d}\right)^2\left(\frac{x}{d}\right)^2\right],$$

$$T_{\mathrm{e}} \equiv T_{\mathrm{ei}}, \quad V \equiv 0, \quad 0 \le x \le d,$$

where n_ε is the peak value of the initial charged particle densities, ε is a small positive number, d is the gap between the parallel-plate electrodes, k_{s} is the electron recombination coefficient, γ is the secondary electron emission coefficient, f_1 and f_2 are the high and low frequencies, and V_1 and V_2 are the applied voltages corresponding to the frequencies.

Our group used a similar model to study the effect of the second electron emission on the plasma characteristics in single radio frequency (RF) capacitive glow discharge at low pressure.[24] Here in this study, we only change the boundary condition on the powered electrode for the applied voltage.

3. Results and discussion

The fluid model is used to study the capacitively coupled RF discharge with and without the metastable atoms. Lymberopoulos and Economou used the model to study the effect of the metastable atoms.[23] Liu *et al.* also used the model to study the effect of the secondary electron emission.[24] Recently, Liu et al. used the model again to compare the continuous and pulse RF glow discharge.[30] In this work, we use the model with similar parameter values to theirs. We study the effect of the pressures (changing from 0.3 Torr to 1.5 Torr) on the plasma characteristics in dual frequency argon capacitive glow discharge.

Uniform meshes are used both in space and in time, and implicit difference schemes are adopted to solve numerically the model. The parameter values used in our computing are given in Table 2.

The results of the discharge evolutions are obtained from our numerical simulation for our model at different gas pressures. Figure 1 shows the electron density evolutions at the position $x = 0.5d$ for different gas pressures during 6000 cycles. From now on, all the cycles are for the high frequency. Based on the results, the discharge process can be divided into three stages: fast growth stage, slow growth stage and steady state stage. It shows that the gas pressure affects both the time of the reaching steady state stage of the discharge and the height of the plasma density when the discharge reaches the steady state stage. With the gas pressure increasing, the time of the reaching steady state stage of the discharge becomes longer. The electron density, when the discharge reaches the steady state stage, increases with increasing gas pressure. This is due to the fact that electrons easily gain energy at lower gas pressure, so that the steady state stage can be reached quickly. A similar result of electron density can be found in the experiment by Yu *et al.*[12] They showed the dependence of electron density on 2-MHz power in dual frequency capacitively coupled plasma with different exciting high frequencies (HFs), with the HF power kept at 40 W and a pressure of 5 Pa.

Table 2. Parameters used in the numerical simulation.

Name	Symbol	Value	Reference
Electron diffusivity/cm^{-1}·s^{-1}	$n_{\rm n}D_{\rm i}$	3.86×10^{22}	[23], [24]
Electron mobility/V^{-1}·cm^{-1}·s^{-1}	$n_{\rm n}\mu_{\rm e}$	9.66×10^{21}	[23], [24]
Ion diffusivity/cm^{-1}·s^{-1}	$n_{\rm n}D_{\rm i}$	2.07×10^{18}	[23], [24]
Ion mobility/V^{-1}·cm^{-1}·s^{-1}	$n_{\rm n}\mu_{\rm i}$	4.65×10^{19}	[23], [24]
Electron recombination coefficient/cm·s^{-1}	$k_{\rm s}$	1.19×10^{7}	[23], [24]
Gap between the electrodes/cm	d	2.5	
High frequency/MHz	f_1	30	
Low frequency/MHz	f_2	2	
Peak voltage of high frequency/V	V_1	100	
Peak voltage of low frequency/V	V_2	20	
Initial electron temperature/eV	$T_{\rm ei}$	1	[23], [24]
Electron temperature at the electrodes/eV	$T_{\rm eb}$	0.5	[23], [24]
Secondary electron coefficient	γ	0.01	[23], [24]

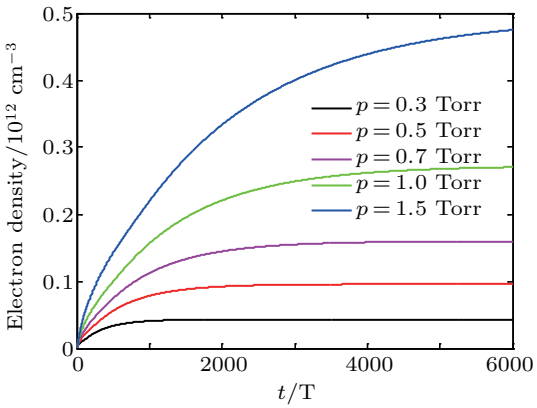


Fig. 1. (color online) Evolutions of electron density at $x = 0.5d$ for the gas pressures of 0.3, 0.5, 0.7, 1.0, and 1.5 Torr during 6000 cycles, respectively. The latter T in abscissa axis represents period (or cycle).

Figure 2 gives the spatial distributions of the cycle-averaged electron densities and ion densities and the cycle-averaged electron densities on the surfaces of the electrodes, at the gas pressures of 0.3, 0.5, 0.7, 1.0, and 1.5 Torr, respectively. From now on, all the cycle-averaged means the averaging in 15 cycles for the high frequency. From Fig. 2(a), the electron densities are higher in the bulk plasma region than in other regions and there are maxima in the middle of the discharge region. From Fig. 2(b), it can be seen that the distributions of the ion density are almost the same as those of electron density in the bulk plasma region, but they have small difference in the sheath regions. Kawamura *et al*. gave the structure of a typical high voltage capacitive dual frequency sheath. They showed that the ions with an initial velocity approximately equal to the Bohm velocity enter into the ion sheath region from the bulk plasma region. Because the ion velocity increases as it approaches to the electrode, so the ion density in the sheath region must decrease due to ion particle conservation.[5]

Figure 2(c) shows the variations of cycle-averaged electron densities on the powered electrode and on the grounded electrode at the low frequency and the high frequency 30 MHz/2 MHz with gas pressure in a range from 0.3 Torr to 1.5 Torr. It is found that the electron densities on powered electrode and on grounded electrode are identical, but the electron density changes much with the gas pressure increasing. The increases of electron density with increasing pressure in dual frequency of 30 MHz/2 MHz show similar results to those presented by Yuan *et al.*, in experiments.[22] In the bulk plasma region, the electron density grows greatly as the gas pressure increases. Both in the powered sheath region and in the grounded sheath region, the electron densities increase slightly as the gas pressure increases. The maximum of the initial electron density is set to be 10^8 cm^{-3}. At the beginning of the RF cycle, the electron density is low and increases linearly between the powered and the grounded electrodes. The secondary electrons are emitted from the surfaces of the powered and the grounded electrodes due to the bombardment of ions. The electrons are accelerated by a strong electric field towards the bulk plasma region. These electrons can contribute to ionization significantly.

Figure 3 shows the spatial distributions of the cycle-averaged ionization rates, at the gas pressures of 0.3, 0.5, 0.7, 1.0, and 1.5 Torr, respectively, in the 6000th cycle. It is known that the ionization rate is dominated by sheath expansion heating. There are two different ionization mechanisms: one is from the electrons emitted by the electrodes and accelerated through the sheath fields, and the other is from the electrons heated by the local electric field.[29] It can be seen that the cycle-averaged ionization rate has one peak in the each sheath region and has another peak in the bulk plasma region. The ionization rate is large in the bulk plasma region due to the penetration of high-energy electrons when the low and high frequencies take effect together.[26–28] Our results are compared with the results in PIC simulation by Zhang *et al.*[20] Because the large sheath potential decreases near the electrode in the former low frequency half-period, the ions are continuously attracted to bombard the electrode. Thus, a significant number of secondary electrons are emitted and accelerated to high energy in the sheath regions. This leads to providing an ionization rate in the sheath region. In dual fre-

quency discharge, a high frequency of the electric field provides a high ionization rate, due to the electron impact and the dense plasma. Whereas the low frequency increases the voltage drop in the sheath regions and accelerates the ions to higher energy.[7] The ionization increases with the increasing gas pressure in the whole discharge region. It has a peak in the middle of the discharge region, and presents an asymmetrical shape. In particular, at the gas pressure ranging from 0.5 Torr to 1.5 Torr, the ionization rate has another peak in each of the powered sheath region and the grounded sheath region. This is because with the increasing of the gas pressure, the density of neutral atoms becomes larger than ones at lower gas pressures although it is difficult for the electrons to gain energy. So the ionization rate rises, then the plasma density increases. The ionization rate in electrically symmetric DF discharge, shown in Fig. 3, is similar to the result in PIC simulation by Schulze *et al.*[16]

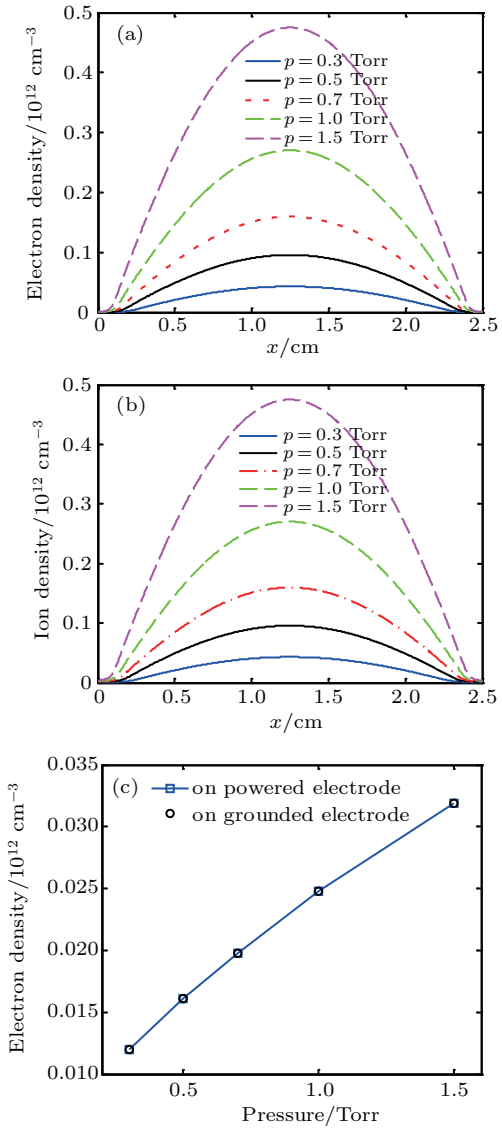


Fig. 2. (color online) Spatial distributions of the cycle-averaged (a) electron density, (b) ion density, (c) electron density on powered electrode and on grounded electrode at the gas pressures of 0.3, 0.5, 0.7, 1.0, and 1.5 Torr in the 6000th cycle, respectively.

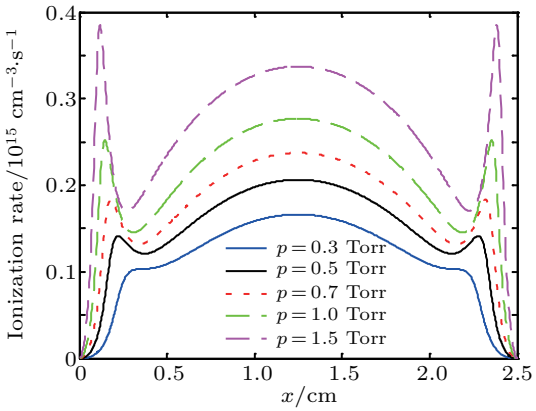


Fig. 3. (color online) Spatial distributions of the cycle-averaged ionization rate at gas pressures of 0.3, 0.5, 0.7, 1.0, and 1.5 Torr in the 6000th cycle.

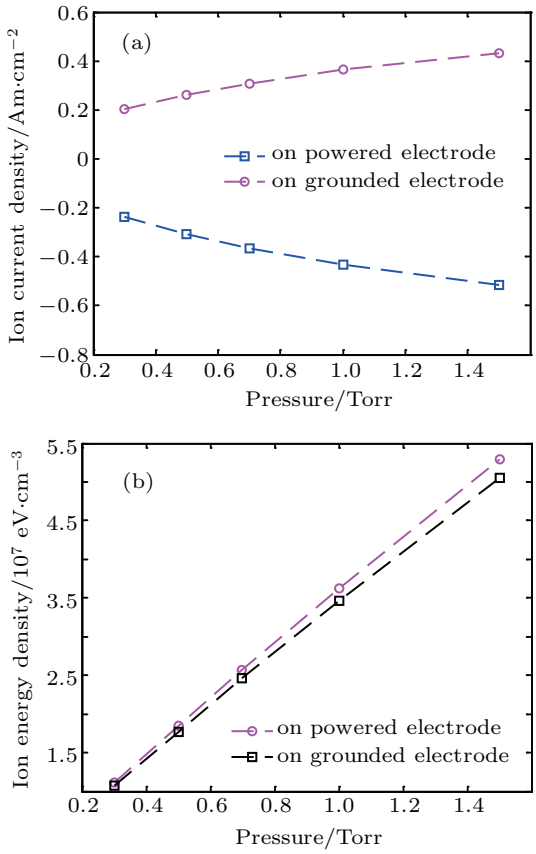


Fig. 4. (color online) Cycle-averaged (a) ion current densities and (b) ion energy densities on powered electrode and on grounded electrode at the gas pressures of 0.3, 0.5, 0.7, 1.0, and 1.5 Torr, respectively, in the 6000th cycle.

On the electrode surfaces, the ion current density and ion energy density are two important parameters for many applications. In order to better understand the ion energy dissipation mechanisms affected by gas pressure, figure 4 presents the cycle-averaged ion current densities and ion energy densities on the surfaces of the powered electrode and the grounded electrode at the gas pressures of 0.3, 0.5, 0.7, 1.0, and 1.5 Torr, respectively, in the 6000th cycle. From Fig. 4(a) the ion current densities are negative on the surface of the powered electrode and increase negatively as gas pressure increases. It shows that the effect of the ion current density on the surface

of the powered electrode increases with increasing gas pressure. Meanwhile, the ion current densities are positive on the surface of the grounded electrode and increase as gas pressure increases. The results show that the effect of the ion current on the surface of the grounded electrode increases with increasing gas pressure. The effect of the increasing gas pressure on the ion current causes the particles to grow more at the electrodes and the secondary electron emissions from electrodes also grow rapidly. The results are that the electron density increases, the width of sheath region decreases and the electric field enlarges as seen in Fig. 7.

Figure 4(b) shows that the ion energy densities increase with increasing gas pressure and the distributions of the ion energy density on the surfaces of the powered electrode and the grounded electrode have small difference. The ions more easily respond to instantaneous low frequency sheath potential, that is why they can gain bigger maximum energy. At higher pressure, the shorter mean free path leads to an increase in the collision frequency between energetic ion and neutral atoms in the ion-atomic charge transferring process. Thus, the more ions, especially the high energetic ions, experience more intensive collisions with neutrals and lose their energy when crossing over the sheath.[10]

Figure 5 shows the variations of the instantaneous electron density in powered sheath region at the gas pressures of 0.3, 0.5, 0.7, 1.0, and 1.5 Torr from the 5970th to the 6000th cycle. From Fig. 1, we can see that the electron density at $x = 0.5$ has no oscillation. But, from Fig. 5, we can see that the electron density has oscillation in the powered sheath region. It is clear that the electron density in the powered sheath region is modulated by both the low-frequency and high-frequency sources. That is to say, the slow oscillations are modulated by the low frequency source, while the fast oscillations are modulated by the high frequency source, so it indicates both the effects between the two frequency sources are very strong.[15] As the gas pressure increases, the amplitude of the oscillation increases and the phase changes. This is because the width of the sheath decreases as pressure increases. Therefore, the responses of the plasma to the RF modulation are different at the same position.

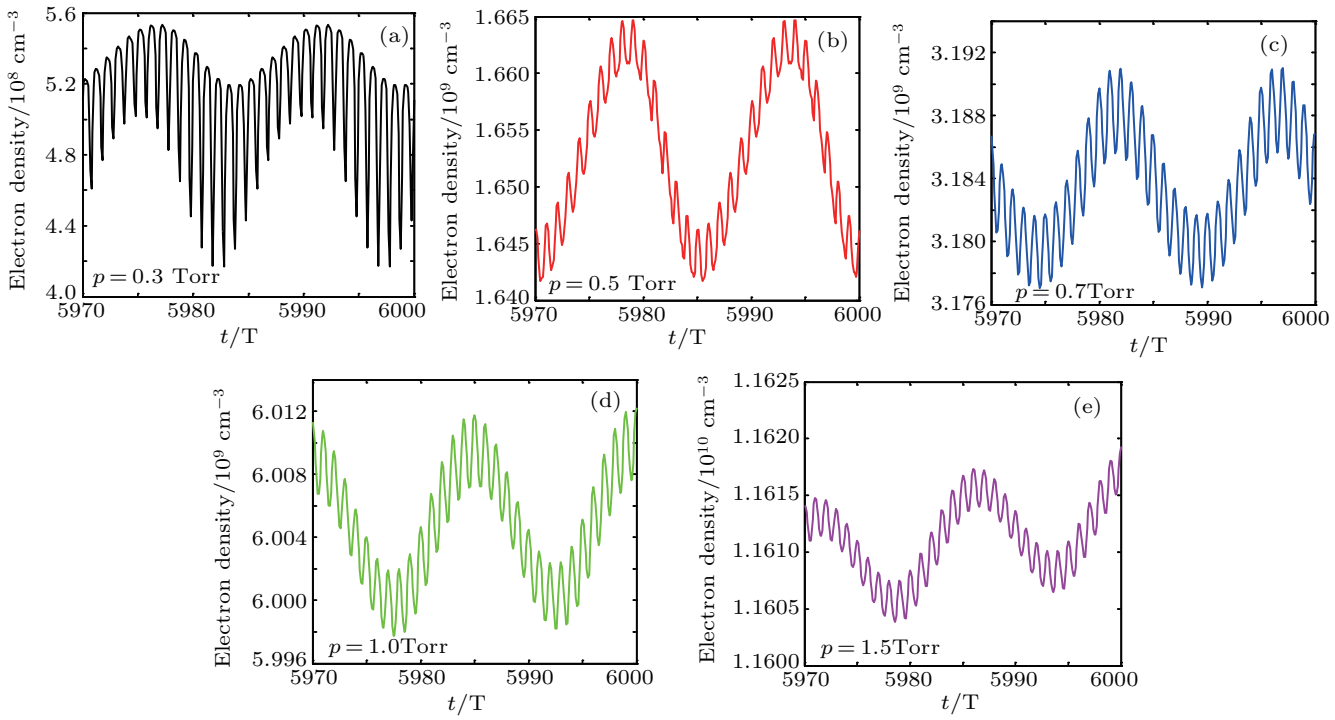


Fig. 5. (color online) Electron densities at $x = 0.1d$ for the gas pressures of (a) 0.3, (b) 0.5, (c) 0.7, (d) 1.0, and (e) 1.5 Torr from the 5970th to the 6000th cycle.

Figure 6(a) gives the spatial distributions of the cycle-averaged electron temperature at the gas pressures of 0.3, 0.5, 0.7, 1.0, and 1.5 Torr, respectively, in the 6000th cycle. It shows that the electron temperature decreases with the increase of gas pressure in the whole discharge region; the electron temperatures in the two sheath regions are higher than in the bulk plasma region; the electron temperature has peak values in the two sheath regions and the width of the peak decreases with increasing gas pressure.

Figure 6(b) presents the maximum electron temperatures in the two sheath regions and the electron temperature in the middle of the discharge region at different gas pressures. The figure shows that the maxima of the electron temperature are not the same in the two sheath regions, the maxima of the electron temperature in powered sheath region and in grounded sheath region are the same. The maximum decreases with increasing gas pressure. In sheath regions, the electron density and electric field are strongly modulated due to the sheath con-

traction and expansion on each electrode successively. The modulations of the electron density and electric field are affected by action of two frequencies. So, the ionization rate will be large in the bulk plasma region due to the penetration of high-energy electrons as shown in Fig. 3.

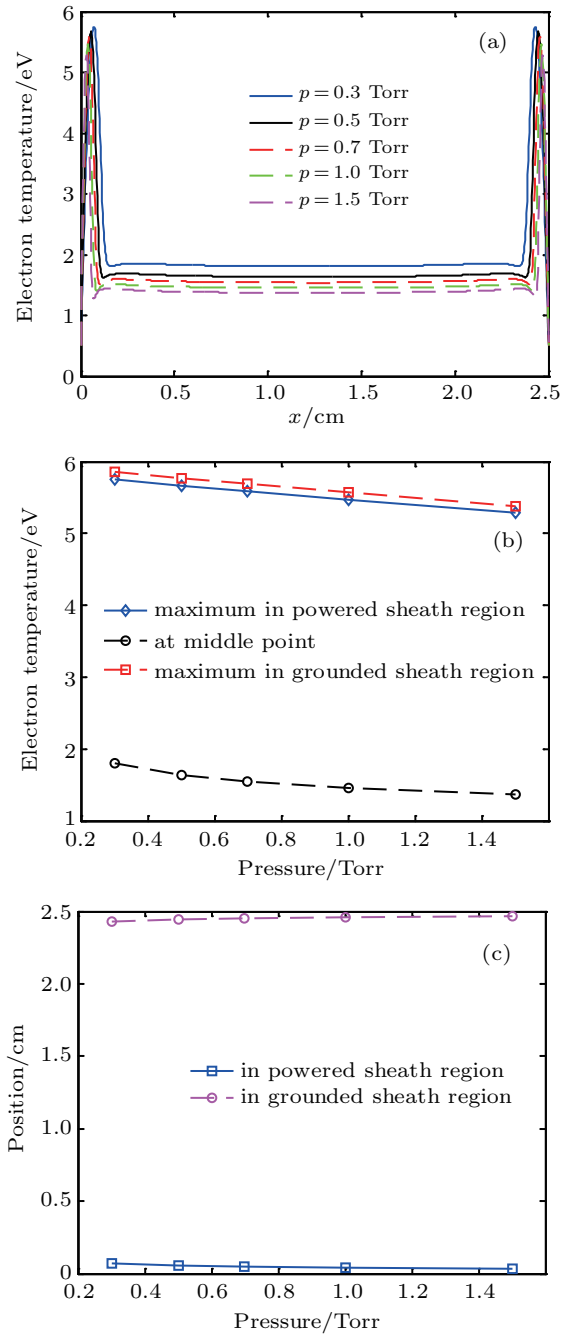


Fig. 6. (color online) (a) Spatial distributions of the cycle-averaged electron temperature, (b) maxima of electron temperature in powered sheath region, in grounded sheath region and electron temperature in the middle of the bulk plasma region, (c) positions of maximum electron temperature in powered sheath region and in grounded sheath region, at the gas pressures of 0.3, 0.5, 0.7, 1.0, and 1.5 Torr, respectively, in the 6000th cycle.

Although the electron temperature is almost constant in the bulk plasma region, and is lower than in the two sheath regions and decreases with increasing gas pressure, the variation of the electron temperature in the whole discharge region is almost the same. The electrons in the bulk plasma region gain energy from the sheath expansion, and electrons emitted from the electrodes are accelerated by the sheath electric field to gain high energies, so that the coupling effect between the two frequency sources is very strong in the sheath but lower in bulk plasma. In Fig. 6, the results of the electron temperatures are similar to the results in the experiment by Yuan *et al.*[22]

Figure 6(c) indicates the positions of the maximum of the electron temperature in the two sheath regions. The corresponding positions in the two sheath regions shift towards the electrodes as the gas pressure increases. The electron temperature in the bulk plasma is mainly determined by the high frequency. The results of Fig. 6(c) are similar to Yu *et al.*'s experimental results.[12]

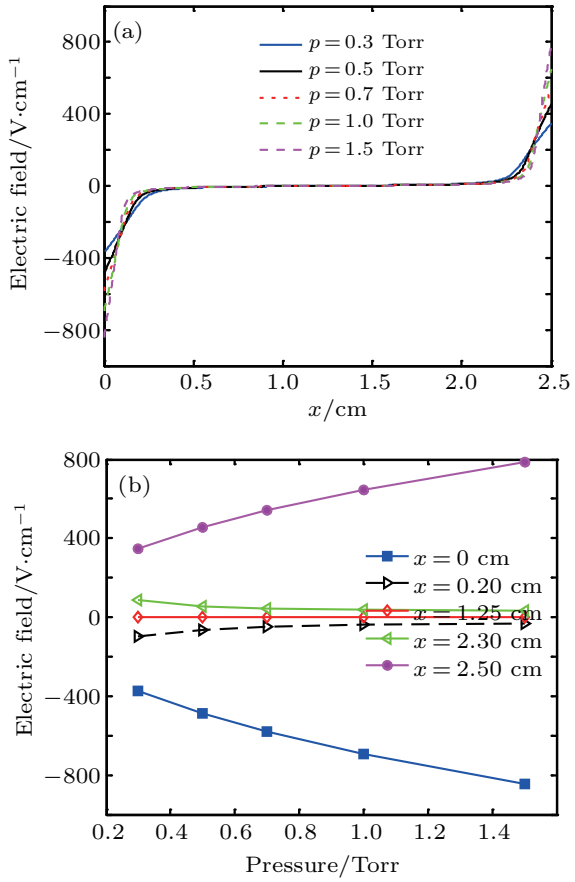


Fig. 7. (color online) (a) Spatial distributions of the cycle-averaged electric field, (b) electric fields at $x = 0.00$ cm, 0.20 cm, 1.25 cm, 2.30 cm, and 2.50 cm, at the gas pressure of 0.3, 0.5, 0.7, 1.0, and 1.5 Torr, respectively, in the 6000th cycle.

Figure 7(a) represents the spatial distributions of the cycle-averaged electric field at the gas pressures of 0.3, 0.5, 0.7, 1.0, and 1.5 Torr, respectively, in the 6000th cycle. The influence of the gas pressure on the electric field is very strong in the two sheath regions. However, in the bulk plasma region, the gas pressure affects the electric field a little and the width of the bulk plasma region increases as the gas pressure increases, due to the changes of the electron and ion densities. The cycle-averaged electric field increases from the negative

peak to zero in the powered sheath region, maintains almost constant zero value in the bulk plasma region, and then increases from zero to its positive maximum in the grounded sheath region. Also, it can be found that the electrons can gain higher energy from the electric field in the two sheath regions. Therefore, the electron temperature has a peak value in the two sheath regions and it is shown in Fig. 6(a).

Figure 7(b) gives the electric fields at positions of $x =$ 0.00 cm, 0.20 cm, 1.25 cm, 2.30 cm, and 2.50 cm at the gas pressures of 0.3, 0.5, 0.7, 1.0, and 1.5 Torr, respectively in the 6000th cycle. Because the electric field presents more variations in the two sheath regions, we choose some special positions symmetrically in order to further study in depth the electric field in the two sheath regions as follows: the positions of $x = 0.00$ cm, 0.20 cm in the powered sheath region, the positions of $x = 2.30$ cm, 2.50 cm in the grounded sheath region, and the position of $x = 1.25$ cm in the middle of the whole discharge region. At the position of $x = 1.25$ cm, the electric field is mainly due to two effective frequencies rather than the plasma density. It shows that the electric field is negative in the powered sheath region, and it increases with increasing gas pressure at $x = 0.00$ cm, whereas it decreases with increasing gas pressure at $x = 0.20$ cm. In the bulk plasma region, it can be seen that the electric field is almost zero. Conversely, the electric field is positive in the grounded sheath region. It increases at $x = 2.50$ cm, but decreases at $x = 2.30$ cm with increasing gas pressure. In the whole discharge region, the changes of the electric field present asymmetrical distribution.

The electron heating of the capacitive discharge at low pressure is a very important process. Liu *et al.* studied the electron heating in capacitive RF argon discharges with single frequency at low pressure by a fluid model.[24] Lafleur *et al.* studied the same problem by the PIC model.[25] In order to further study the gaining and losing of electron energy during the discharge, the cycle-averaged results of the electron pressure heating, the electron ohmic heating, the electron heating and the electron energy loss in dual frequency argon capacitive glow discharges at the gas pressures of 0.3, 0.5, 0.7, 1.0, and 1.5 Torr, respectively, in the 6000th cycle are given in Fig. 8.

Figure 8(a) shows that the cycle-averaged electron pressure heating is negative in the whole discharge region. From Eq. (14), the electron pressure heating is from the gradients of the electron density and the electric field. Figure 2(a) shows that the gradient of the electron density in the powered sheath region is large and positive, and the gradient of the electron density increases as the gas pressure increases. Figure 7(a) shows that the electric field in the powered sheath region is large and negative, and the electric field increases negatively as the gas pressure increases. Thus, in the powered sheath region, the electron pressure heating becomes negative, increases negatively as the gas pressure increases, and it has a negative peak. Meanwhile, figure 2(a) shows that the gradient of the electron density in the grounded sheath region is large and negative, and the gradient of the electron density increases negatively as the gas pressure increases. Figure 7(a) shows that the electric field in the grounded sheath region is large and positive, and the electric field increases as the gas pressure increases. Thus, in the grounded sheath region, the electron pressure heating becomes negative, increases negatively as the gas pressure increases, and it has a negative peak too. In Fig. 2(a), we can find that the gradient of the electron density is small in the bulk plasma region. In Fig. 7(a), we can see that the electric field is almost zero in the bulk plasma region. So, in the bulk plasma region, the electron pressure heating is very small. Figure 8(a) shows that in the whole discharge region, the electron pressure heating is negative, increases negatively as the gas pressure increases, and it takes place mainly in the two sheath regions. The position of the peak in each sheath region shifts towards the electrode as the gas pressure increases. The results indicate that the cycle-averaged effect of the electron pressure heating on the electrons is 'cooling'.

When the sheath expansion is quick enough, if the high frequency is sufficiently large, the electrons can gain energy and ionize the neutral gas. When the sheath expansion is slow, if the low frequency is large enough, the electrons can loss energy and ionize a small quantity of neutral gas. According to Fig. 8(b), the results show that the cycle-averaged electron ohmic heating has positive values in the whole discharge region because the ion current is accelerated across the sheath.[26] The peaks of electron ohmic heating are found in the two sheath regions, and they increase as the gas pressure increases. From Eq. (15), the electron ohmic heating is from the electron density and the square of the electric field. It can be seen that the electron density in Fig. 2(a) and the square of the electric field in Fig. 7(a) are both positive and increase with increasing gas pressure in the whole discharge region. The effect of the electron ohmic heating on the electrons is always 'heating' in the whole discharge region and it takes place mainly in the two sheath regions. The electron ohmic heatings in the sheath regions are large because a large number of electrons are accelerated by the electric fields in the sheath regions compared with in the bulk plasma region.

The electron heating plays a crucial role in electron energy deposition and is sum of the electron pressure heating and the electron Ohmic heating together from Eq. (13). From Fig. 8(b), the electron Ohmic heating is positive in the whole discharge region. While from Fig. 8(a), the electron pressure heating is negative in the whole discharge region. Figure 8(c) shows that the electron heating mainly occurs in the two sheath regions, with a small constant value in the bulk plasma region. It indicates that in the whole discharge region, the electron Ohmic heating is stronger than the electron pres-

sure heating. However, since the signs of two mechanisms are opposite, they cancel out. The effect increases as the gas pressure increases. However, near the two electrodes, the electron heating becomes negative. It indicates that the electron pressure heating is stronger than the electron ohmic heating near the two electrodes. The effects of the dual frequency in the electron heating are as follows: the effect of the low frequency electron power is largest near electrodes but the effect of the high frequency electron power is largest near boundaries between the bulk plasma region and the sheath regions. So, the electron heating is mainly contributed from the high frequency electron power. The low frequency electron power in the sheath increases more as the gas pressure increases due to the additional heating of secondary electrons, so the total electron heating near electrodes becomes positive.

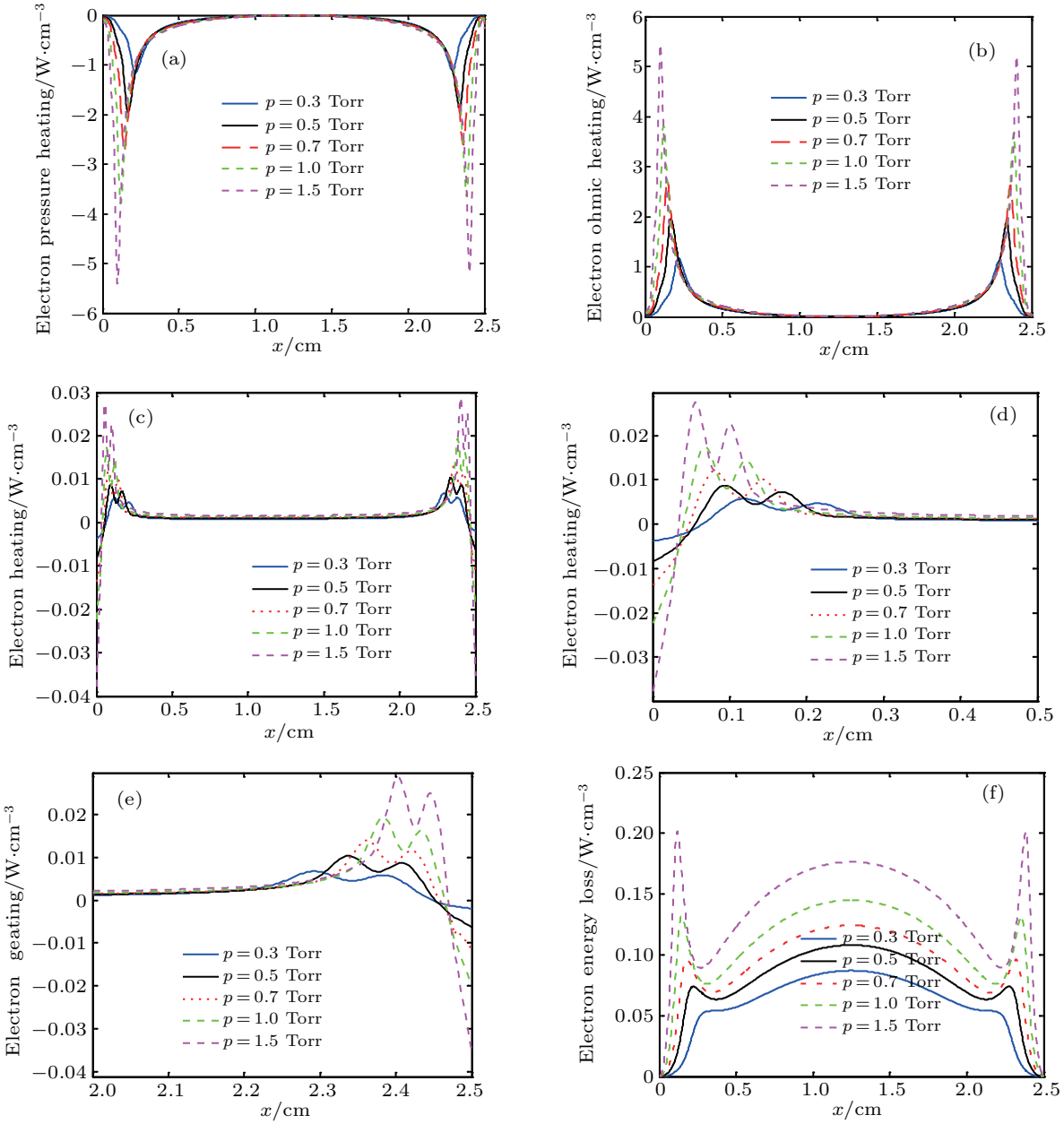


Fig. 8. (color online) Spatial distributions of the cycle-averaged (a) electron pressure heating, (b) electron ohmic heating, (c) electron heating in all the discharge regions, (d) electron heating in powered sheath region, (e) electron heating in grounded sheath region, (f) electron energy loss, at the gas pressures of 0.3, 0.5, 0.7, 1.0, and 1.5 Torr, respectively, in the 6000th cycle.

Figures 8(d) and 8(e) show double peaks of the electron heating in the sheath regions, because high energy secondary electrons lead to the severe collisions near the electrodes, and the interaction between the energetic electrons and the oscillation sheath brings about the drastic collisions near the boundaries between the bulk plasma and the sheaths. The generating double peaks of the electron heating both in the grounded sheath region at the period time $t = (1/4)$ cycle and in the powered sheath region at the period time $t = (3/4)$ cycle are all found in PIC simulation results as indicated by spatiotemporal plots of the electron heating rate presented by Schulze *et al.*[28] It has been observed that at the beginning of the RF

cycle the plasma sheath expands, and as a result, the energetic electrons are generated. The pressure effect enhances the generation of the high energetic electrons due to the rapid expansion of the sheath. These electrons travel from the sheath region, propagate through the bulk plasma region and enhance the total plasma current. As pressure increases, the electrical field which heats the electrons and enhances the discharge current increases in the plasma region.

Figure 8(f) shows the influence of the gas pressure on the electron energy loss. As the gas pressure increases, the electron energy loss increases in the whole discharge region. This is due to the higher ionization rate resulting from the higher gas pressure, which increases the electron energy loss both in the two sheath regions and in the bulk plasma region. It results in a small boom at the gas pressure of 0.3 Torr and in a big boom at the gas pressure of 1.5 Torr, occurring in the two sheath regions.

4. Conclusions

A self-consistent fluid model is established to describe the plasma in dual frequency argon capacitive glow discharges at low pressure. Numerical results are obtained from the model by using a finite difference method. From analyses of the results, some conclusions are obtained below.

(i) The evolution of the electron density and the generation of the plasma are affected by low and high frequency as the gas pressure increases. At the middle point of the discharge region, the electron density has no oscillation. However, in the sheath region, the electron density has oscillation and the amplitude of the oscillation increases as pressure increases. Also, the phase of the oscillation is affected strongly by pressure.

(ii) The cycle-averaged plasma density is asymmetric due to the effect of the dual radio frequency. The plasma density increases and becomes more symmetric as gas pressure increases.

(iii) The cycle-averaged ion current density and ion energy density on the electrodes increase as gas pressure increases.

(iv) The cycle-averaged electric field shows a more complex variation behavior as gas pressure changes. The gas pressure affects mainly the electric field in the sheath region. As the gas pressure increases, the width of the sheath decreases and the electric field in the sheath region increases.

(v) The change of the gas pressure has great influences on ionization rate and the electron energy transferring. As the gas pressure increases, the ionization rate increases and becomes symmetric. The electron pressure heating, the electron ohmic heating, the electron heating and the electron energy loss increase as pressure increases. Furthermore, the electron heating has two prominent peaks in each sheath region.

Acknowledgment

The authors would like to thank Miss Qian Liu for her useful discussion, and also wish to thank Dr. Ruiqiang Liu for his helpful advice.

References

[1] Kim H C, Lee J K and Shon J W 2003 *Phys. Plasmas* **10** 4545
[2] Lieberman M A and Lichtenberg A J 1994 *Principles of Plasma Discharges and Material Processing* (New York: Wiley)
[3] Kim H C and Lee J K 2005 *Phys. Plasmas* **12** 053501
[4] Georgieva V and Bogaerts A 2005 *J. Appl. Phys.* **98** 023308
[5] Kawamura E, Lieberman M A and Lichtenberg A J 2006 *Phys. Plasmas* **13** 053506
[6] Liu Y X, Zhang Q Z, Jiang W, Hou L J, Jiang X Z, Lu W Q and Wang Y N 2011 *Phys. Rev. Lett.* **107** 055002
[7] Lisovskiy V, Booth J P, Landry K, Douai D, Cassagne V and Yegorenkov V 2008 *Plasma Sources Sci. Technol.* **17** 025002
[8] Schulze J, Schüngel E, Czarnetzki U and Donkó Z 2009 *J. Appl. Phys.* **106** 063307
[9] Kim D B, Moon S Y and Jung H, Gweon B and Choec W 2010 *Phys. Plasmas* **17** 053508
[10] Li Z C, Chang D L, Li X S, Bi Z H, Lu W Q, Xu Y, Zhu A M and Wanga Y N 2010 *Phys. Plasmas* **17** 033501
[11] Jiang X Z, Liu Y X, Lu W Q, Bi Z H, Gao F and Wang Y N 2012 *Vacuum* **86** 881
[12] Yu Y Q, Xin Y, Lu W Q and Ning Z Y 2011 *Plasma Sci. Technol.* **13** 571
[13] Jiang W, Mao M and Wang Y N 2006 *Phys. Plasmas* **13** 113502
[14] Bora B 2015 *Phys. Plasmas* **22** 103503
[15] Wang S, Xu X and Wang Y N 2007 *Phys. Plasmas* **14** 113501
[16] Schulze J, Derzsi A and Donkó Z 2011 *Plasma Sources Sci. Technol.* **20** 045008
[17] Dai Z L, Xu X and Wang Y N 2007 *Phys. Plasmas* **14** 013507
[18] Donkó Z and Petrovic Z L 2007 *J. Phys.: Conf. Ser.* **86** 012011
[19] Bi Z H, Dai Z L, Xu X, Li Z C and Wang Y N 2009 *Phys. Plasmas* **16** 043510
[20] Zhang Q Z, Liu Y X, Jiang W, Bogaerts A and Wang Y N 2013 *Plasma Sources Sci. Technol.* **22** 025014
[21] Yuan Q H, Xin Y, Yin G Q, Huang X J, Sun K and Ning Z Y 2008 *J. Phys. D: Appl. Phys.* **41** 205209
[22] Yuan Q H, Yin G Q, Xin Y and Ning Z Y 2011 *Phys. Plasmas* **18** 053501
[23] Lymberopoulos D P and Economou D J 1993 *J. Appl. Phys.* **73** 3668
[24] Liu Q, Liu Y, Samir T and Ma Z S 2014 *Phys. Plasmas* **21** 083511
[25] Lafleur T, Chabert P and Booth J P 2014 *Plasma Sources Sci. Technol.* **23** 035010
[26] Gahan D and Hopkins M B 2006 *J. Appl. Phys.* **100** 043304
[27] Turner M M and Chabert P 2006 *Phys. Rev. Lett.* **96** 205001
[28] Schulze J, Derzsi A, Dittmann K, Hemke T, Meichsner J and Donko'Z 2011 *Phys. Rev. Lett.* **107** 275001
[29] Belenguer P and Boeuf J P 1990 *Phys. Rev. A* **41** 4447
[30] Liu R Q, Liu Y, Jia W Z and Zhou Y W 2017 *Phys. Plasmas* **24** 013517
[31] Semmler E, Awakowicz P and Keudell A V 2007 *Plasma Sources Sci. Technol.* **16** 839